Investigation of Lithium Plating-Stripping Process in Li-Ion Batteries at Low Temperature Using an Electrochemical Model

Article *in* Journal of The Electrochemical Society · January 2018

DOI: 10.1149/2.0661810jes

CITATIONS
8

READS
1,420

8 authors, including:

Dongsheng Ren
Tsinghua University
24 PUBLICATIONS **172** CITATIONS
SEE PROFILE

Dongxu Guo
Tsinghua University
6 PUBLICATIONS **10** CITATIONS
SEE PROFILE

Xuebing Han
Tsinghua University
47 PUBLICATIONS **2,976** CITATIONS
SEE PROFILE

Xuning Feng
Tsinghua University
74 PUBLICATIONS **1,242** CITATIONS
SEE PROFILE

Journal of The Electrochemical Society, **165** (10) A2167-A2178 (2018)
0013-4651/2018/165(10)/A2167/12/$37.00 © The Electrochemical Society

Investigation of Lithium Plating-Stripping Process in Li-Ion Batteries at Low Temperature Using an Electrochemical Model

Dongsheng Ren,[1,z] Kandler Smith,[2,*] Dongxu Guo,[1,3] Xuebing Han,[1] Xuning Feng,[1,4,*] Languang Lu,[1] Minggao Ouyang,[1,z] and Jianqiu Li[1]

[1]*State Key Laboratory of Automotive Safety and Energy, Tsinghua University, Beijing 100084, People's Republic of China*
[2]*National Renewable Energy Laboratory, Golden, Colorado 80401, USA*
[3]*Department of Automation, Tsinghua University, Beijing 100084, People's Republic of China*
[4]*Institute of Nuclear and New Energy Technology, Tsinghua University, Beijing 100084, People's Republic of China*

Lithium plating leads to severe capacity fading and possible safety problems in lithium-ion batteries. Thus, non-destructive detection methods for lithium plating are critical for safe and reliable operation of lithium-ion batteries. In this paper, an electrochemical model incorporated with lithium plating and stripping reactions is established to investigate the lithium plating-stripping process at low temperature. The model is validated at different current rates and temperatures and can successfully predict the characteristic voltage plateau during the rest period after low temperature charging. Modeling analysis helps to develop detection method for lithium plating via differential analysis on the voltage plateau. Distinct local minima can be found in the differential voltage curves of the batteries with plated lithium. The time when the local minima occurs in the differential voltage curves exhibits a linear relationship with the amount of reversible lithium, and thus can be applied as a quantitative indicator for detection of lithium plating. The detection of lithium plating based on differential voltage analysis is further extended to the discharge voltage profiles of the batteries after low temperature charging, considering the effects of rest time.
 [DOI: 10.1149/2.0661810jes]

Manuscript submitted April 24, 2018; revised manuscript received July 5, 2018. Published July 14, 2018.

Lithium-ion batteries have been widely used in electric vehicles (EVs) and play an important role in the improvement of the EVs' performance, considering their high energy density and prolonged cycle life.[1] However, lithium-ion batteries still suffer from various aging mechanisms,[2] such as lithium plating, solid electrolyte interphase (SEI) film growth and loss of active material at cathode and anode, which reduce battery capacity and might cause safety problem.[3,4]

Lithium plating is one of the most severe aging process in lithium-ion batteries using graphite as anode material.[3,5] The plated lithium metal will react with electrolyte to thicken SEI film, resulting in capacity loss and internal resistance increase.[3,5,6] Lithium plating will also have impacts on battery safety performance. Batteries with lithium metal plated at anode were found to exhibit a much lower onset temperature (less than 50°C) of exothermic reactions and larger heat generation between 50°C and 100°C compared to fresh batteries.[7–9] Moreover, metallic lithium can grow dendritically and pierce separator to cause internal short circuit,[10,11] which can initiate thermal runaway. Therefore, lithium plating should be effectively prevented or detected to ensure safe and reliable operation of lithium-ion batteries.

Electrochemical experiments and post-mortem analysis have been conducted to reveal the lithium plating mechanism in lithium-ion batteries,[12–14] with the help of some in-situ and non-destructive methods, such as lithium reference electrode,[12,14] in-situ neutron diffraction,[15,16] in-situ ^{7}Li nuclear magnetic resonance (NMR),[17–19] and time-resolved operando electron paramagnetic resonance (EPR).[20] Lithium plating will occur at anode surface when the anode overpotential drops below 0V vs. Li/Li$^+$ due to liquid or solid phase mass transfer limitation or limited charge transfer kinetics of the lithium intercalation reaction,[21] which are favored by low temperature charging,[5,6] fast charging[22] or overcharging.[23] In general, part of the plated lithium will be consumed irreversibly due to the reaction with electrolyte to form new SEI film or the formation of "dead" lithium that is electrically isolated with anode, while most of the plated lithium is reversible.[20] Reversible lithium, which is still in electrical contact with the anode - can undergo charge transfer reaction into electrolyte and then re-intercalate into anode, and the whole process is known as lithium stripping process. The stripping of the plated lithium was observed to happen during the rest or discharge period after lithium plating,[20] resulting a high voltage plateau, which can be considered as an effective indicator for lithium plating detection. Some researchers have proposed some quantitative estimation methods for the amount of plated lithium based on differential analysis of the voltage plateau.[15,24,25]

Electrochemical models are crucial in understanding the lithium plating-stripping process and can help to find possible solutions to prevent or detect lithium plating. Arora et al.[26] has incorporated the lithium plating reaction as a side reaction into the pseudo two-dimensional (P2D) model developed by Doyle and Newman,[27,28] and presented the first electrochemical model to investigate the effect of battery design parameters on lithium plating behaviors during overcharge process. An extended two-dimensional model was developed by Tang et al.[29] to study the edge effects on lithium plating reaction. Lithium plating models for low temperature charging were presented in Refs. 30 and 31 to determine the operating limits of lithium-ion batteries at low temperature. Yang et al.[32] has investigated the long-term lithium plating induced aging behaviors by incorporating the SEI growth reaction and lithium plating reaction into the P2D model. Moreover, control-oriented reduced-order lithium plating models have also been established to develop optimal charging algorithms for lithium-ion batteries.[33–37] However, those existing models mainly focused on the lithium plating reactions and assumed the plated lithium to be totally irreversible by neglecting the stripping of reversible lithium, which accounts for the major part of the plated lithium.[20] That leads to errors in determination of the lithium plating conditions and underestimation of the amount of plated lithium. Therefore, electrochemical models incorporated with both lithium plating and stripping reactions should be developed to fully understand the lithium plating-stripping process.

In this study, an electrochemical model incorporated with both lithium plating and stripping reactions is first established. The model is validated with experiments at different current rates and temperatures and can successfully predict the characteristic plateau in the voltage relaxation profiles after low temperature charging. Modeling analysis is conducted to study the origin of the voltage plateau and develop a quantitative detection method for lithium plating.

The Lithium Plating-Stripping Process

In this study, lithium plating and stripping reactions are considered as side reactions in the electrochemical model. Thus, three electrochemical reactions would occur at anode surface during low temperature charging process, as presented in Eq. 1∼3, with the reaction current of each reaction denoted as j_1, j_2 and j_3, respectively. z_1, z_2 and

*Electrochemical Society Member.
[z]E-mail: rds14@mails.tsinghua.edu.cn; ouymg@tsinghua.edu.cn

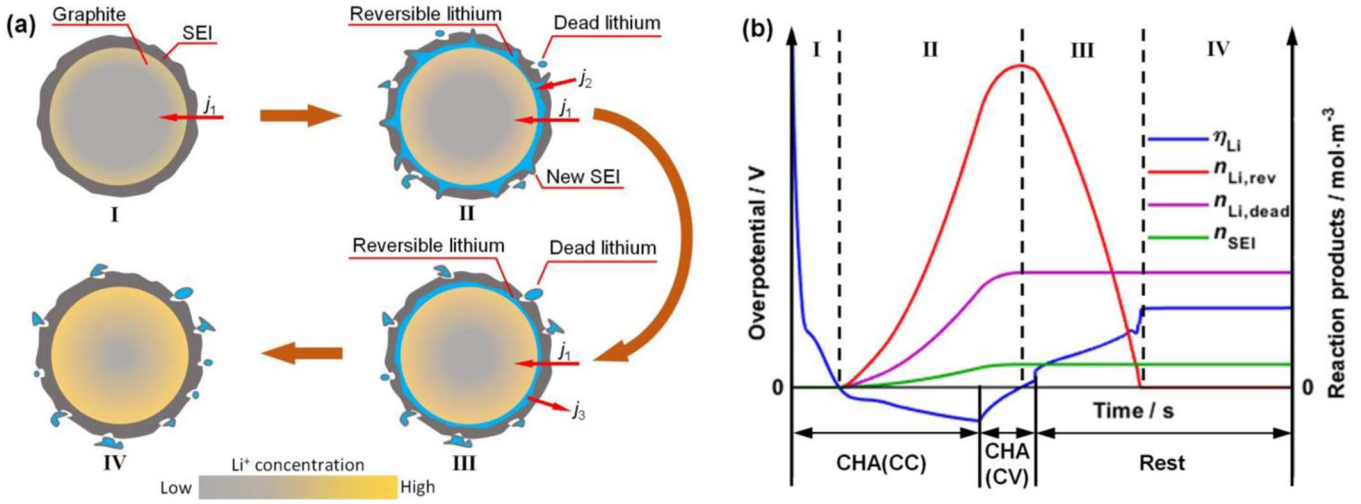

Figure 1. Illustration of the lithium plating-stripping process. (a) four stages during low temperature charging and subsequent rest period; (b) changes of the overpotential η_{Li} and the amount of reaction products.

z_3 are the fractions of the three products generated by lithium plating reaction, respectively. The values of z_1, z_2 and z_3 are modified from those reported in Ref. 20 to fit the experimental data in this study. The total current density j is the sum of three reaction currents, as in Eq. 4.

$$Li_xC_6 + \Delta x Li^+ + e^- \rightarrow Li_{x+\Delta x}C_6 \quad [1]$$

$$Li^+ + e^- \rightarrow z_1\, Li^{(s)}_{rev} + z_2 Li^{(s)}_{dead} + z_3 SEI \quad [2]$$

$$Li^{(s)}_{rev} \rightarrow Li^+ + e^- \quad [3]$$

$$j = j_1 + j_2 + j_3 \quad [4]$$

The low temperature charging and subsequent rest process can be divided into four stages according to the reactions happening in the anode, as illustrated in Fig. 1. The electrochemical reactions in each stage are summarized as follows:

Stage I: The desired reaction, i.e. lithium intercalation reaction, happens in the anode at this stage, as presented Fig. 1a. The overpotential of lithium plating reaction η_{Li} is still larger than 0V vs. Li/Li^+ (as in Fig. 1b) and thus no lithium plates at Stage I.

Stage II: Lithium plating reaction begins at Stage II as η_{Li} goes below 0V due to significant polarization, as presented in Fig. 1b. The lithium intercalation reaction current j_1 and lithium plating reaction current j_2 have a same direction and compete with each other at this stage, as illustrated in Fig. 1a. The products of lithium plating reaction are new SEI film, dead lithium and reversible lithium, as show in Fig. 1a. The new SEI film and dead lithium are considered to form immediately during the lithium plating reaction for simplification, as in Eq. 2, neglecting the complex reactions for the generations of SEI film and dead lithium.[38] The rate of lithium plating reaction is determined by the overpotential η_{Li}, and the amount of the reaction products (reversible lithium, dead lithium and SEI film) continues to increase until η_{Li} goes higher than 0V, as shown in Fig. 1b.

Stage III: At stage III, lithium stripping reaction occurs as the overpotential η_{Li} goes higher than 0V during constant voltage(CV) charge or rest period. The lithium stripping reaction has the same kinetics as the lithium plating reaction. Only the reversible lithium is consumed in the lithium stripping reaction, while the dead lithium and SEI film are irreversible. The lithium stripping reaction stops when the reversible lithium is fully consumed, as presented in Fig. 1b. At Stage III, the lithium intercalation reaction continues in the anode, and the intercalation reaction current j_1 and lithium stripping reaction current j_3 have opposite directions, as shown in Fig. 1a.

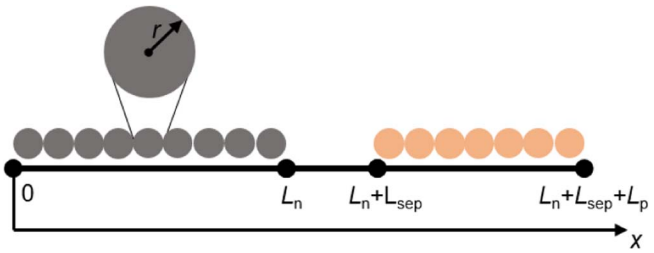

Figure 2. Schematic of the P2D model for lithium-ion batteries.

Stage IV: All the electrochemical reactions stop at this stage, and only diffusion process continues to make the battery reach an equilibrium.

Model Development

An electrochemical model incorporated with both lithium plating and stripping reactions is developed in this research based on the P2D model by Doyle and Newman et al.,[27,28] as presented in Fig. 2. The governing equations in the electrochemical model are listed as follows:

Charge balance equations.—The charge balance in the solid phase follows the Ohm's law, as in Eq. 5. σ^{eff} is the effective electrical conductivity in the solid phase; ϕ_s is the electrical potential in the solid phase; a_s is the specific interfacial area of the particle; F is the Faraday constant; j is the current density. At the external boundaries ($x = 0$, L_n+L_{sep}+L_p), the charge flux is set to be equal to the applied current density i_{app}, as shown in Eq. 6, while there is no charge flux at the inner boundaries ($x = L_n$, L_n+L_{sep}), as in Eq. 7,

$$\frac{\partial}{\partial x}\left(\sigma^{eff}\frac{\partial}{\partial x}\phi_s\right) - a_s F j = 0 \quad [5]$$

$$-\sigma^{eff}\frac{\partial}{\partial x}\phi_s\Big|_{x=0} = -\sigma^{eff}\frac{\partial}{\partial x}\phi_s\Big|_{x=L_n+L_{sep}+L_p} = i_{app} \quad [6]$$

$$\frac{\partial}{\partial x}\phi_s\Big|_{x=L_n} = \frac{\partial}{\partial x}\phi_s\Big|_{x=L_n+L_{sep}} = 0 \quad [7]$$

The potential drop in the electrolyte phase is given by Eq. 8, where κ^{eff} is the effective electrical conductivity in the electrolyte phase; ϕ_e

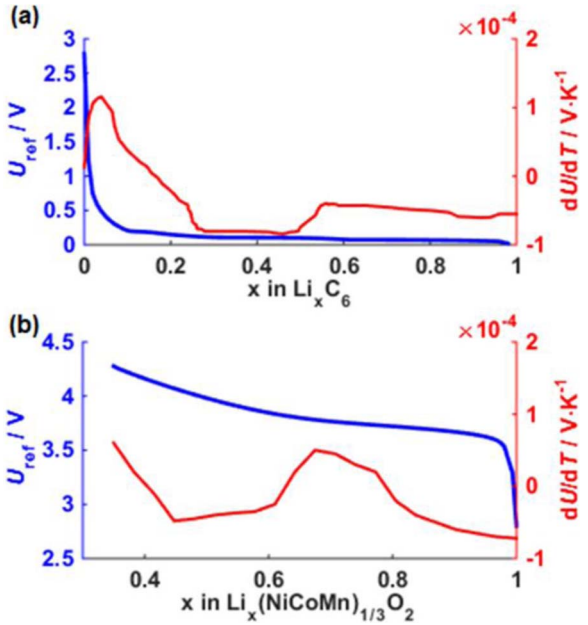

Figure 3. The variations of open circuit potential U_{ref} and the entropic heat coefficient $\frac{dU}{dT}$ with the stoichiometric coefficients x. (a) negative electrode; (b) positive electrode.

is the electrical potential in the electrolyte phase; R is the gas constant; T is the battery temperature; t_+ is the transference number of Li^+; and c_e is the Li^+ concentration in the electrolyte. ϕ_e is continuous at the inner boundaries ($x = L_n$, L_n+L_{sep}), while it is set to be isolate at the external boundaries since the flux of Li^+ in the electrolyte phase is 0 at $x = 0$, $L_n+L_{sep}+L_p$, as in Eq. 9.

$$\frac{\partial}{\partial x}\left(\kappa^{\text{eff}}\frac{\partial}{\partial x}\phi_e\right)+\frac{2RT(t_+-1)}{F}\frac{\partial}{\partial x}\left(\kappa^{\text{eff}}\frac{\partial}{\partial x}\ln c_e\right)+a_s F j=0 \quad [8]$$

$$\left.\frac{\partial}{\partial x}\phi_e\right|_{x=0}=\left.\frac{\partial}{\partial x}\phi_e\right|_{x=L_n+L_{sep}+L_p}=0 \quad [9]$$

Mass balance equations.—The mass balance of Li^+ in a spherical particle of electrode active materials is described by Fick's law, as in Eq. 10. c_s is the solid phase concentration of Li^+ in the particle, D_s is the solid phase diffusion coefficient, and R_s is the radius of the particle. The flux of Li^+ at the center of the particle ($r = 0$) is 0, as in Eq. 11, because there is no lithium source; while the flux at the surface ($r = R_s$) is determined by the current density of the electrochemical reactions, as in Eq. 12.

$$\frac{\partial c_s}{\partial t}-\frac{D_s}{r^2}\frac{\partial}{\partial r}\left(r^2\frac{\partial c_s}{\partial r}\right)=0 \quad [10]$$

$$\left.D_s\frac{\partial c_s}{\partial r}\right|_{r=0}=0 \quad [11]$$

$$\left.D_s\frac{\partial c_s}{\partial r}\right|_{r=R_s}=-j \quad [12]$$

The Li^+ concentration distribution in the electrolyte phase follows Eq. 13. ε_e is the volume fraction of the electrolyte phase, and D_e^{eff} is the effective electrolyte phase diffusion coefficient. The flux of Li^+ in the electrolyte phase is set as 0 at the external boundaries ($x = 0$, $L_n+L_{sep}+L_p$), as shown in Eq. 14, while the Li^+ concentration at inner boundaries ($x = L_n$, L_n+L_{sep}) are taken to be continuous.

$$\frac{\partial}{\partial t}(\varepsilon_e c_e)=\frac{\partial}{\partial x}\left(D_e^{\text{eff}}\frac{\partial}{\partial x}c_e\right)+(1-t_+)a_s j \quad [13]$$

$$\left.\frac{\partial}{\partial x}c_e\right|_{x=0}=\left.\frac{\partial}{\partial x}c_e\right|_{x=L_n+L_{sep}+L_p}=0 \quad [14]$$

Electrochemical kinetics equations.—For the lithium intercalation reaction in cathode and anode, the local current density per active material area is calculated by the Butler-Volmer equation, as in Eq. 15, where $i_{0,1}$ is the exchange current density and can be derived from Eq. 16 according to the reaction kinetics, k_1 is the reaction rate constant, and $\alpha_{a,1}$ and $\alpha_{c,1}$ are the anodic and cathodic transfer coefficients, respectively. η_1 is the reaction overpotential and can be calculated by Eq. 17. U is the thermodynamic equilibrium potential of the solid phase and can be calculated by Eq. 18, where U_{ref} is the open circuit potential at reference temperature $T_{\text{ref}} = 298.15$K, and $\frac{dU}{dT}$ is the entropic heat coefficient. FjR_{SEI} represents the potential loss due to the SEI film, where R_{SEI} is the resistance of SEI film, and j is the total local current density and equals j_1 in cathode, while j in anode is calculated by Eq. 4.

$$j_1=i_{0,1}\cdot\left[\exp\left(\frac{\alpha_{a,1}F\eta_1}{RT}\right)-\exp\left(\frac{\alpha_{c,1}F\eta_1}{RT}\right)\right] \quad [15]$$

$$i_{0,1}=k_1\cdot c_e^{\alpha_{a,1}}(c_{s,\max}-c_{s,\text{surf}})^{\alpha_{a,1}}c_{s,\text{surf}}^{\alpha_{c,1}} \quad [16]$$

$$\eta_1=\phi_s-\phi_e-U-FjR_{SEI} \quad [17]$$

$$U=U_{\text{ref}}(x)-(T-T_{\text{ref}})\frac{dU}{dT} \quad [18]$$

According to Arora et al.,[26] the rate of lithium plating reaction also follows the Butler-Volmer equation, as in Eq. 19, where the exchange current density $i_{0,2}$ is calculated by Eq. 20. The overpotential η_{Li} is calculated by Eq. 21 with the equilibrium potential of lithium plating reaction U_{Li} considered as 0V. The lithium stripping reaction has the same kinetics as lithium plating reaction, and the reaction rate can be calculated by Eq. 22, where $\frac{\beta\cdot n_{Li,rev}}{1+\beta\cdot n_{Li,rev}}$ is the correction term considering the limitation by the amount of reversible lithium $n_{Li,rev}$. β is a large value to effectively make the term $\frac{\beta\cdot n_{Li}}{1+\beta\cdot n_{Li}}$ equal to 1 when $n_{Li,rev} >> 1$, and 0 when $n_{Li,rev} = 0$, as in Ref. 39,40

$$j_2=i_{0,2}\cdot\left[\exp\left(\frac{\alpha_{a,2}F\eta_{Li}}{RT}\right)-\exp\left(\frac{\alpha_{c,2}F\eta_{Li}}{RT}\right)\right],\ \eta_{Li}<0 \quad [19]$$

$$i_{0,2}=k_2\cdot c_e^{\alpha_{a,2}} \quad [20]$$

$$\eta_{Li}=\phi_s-\phi_e-U_{Li}-FjR_{SEI} \quad [21]$$

$$j_3=i_{0,2}\cdot\left[\exp\left(\frac{\alpha_{a,2}F\eta_{Li}}{RT}\right)-\exp\left(\frac{\alpha_{c,2}F\eta_{Li}}{RT}\right)\right]\cdot\frac{\beta\cdot n_{Li,rev}}{1+\beta\cdot n_{Li,rev}},\quad \eta_{Li}>0\ \&\ n_{Li,rev}>0 \quad [22]$$

As illustrated in Fig. 1, the SEI film will be thickened due to lithium plating, resulting in increase of R_{SEI}, as in Eq. 23, where σ_{SEI} is the electrical conductivity of the SEI film, $\delta_{SEI,0}$ and $\Delta\delta_{SEI}$ are the original and increased thickness of the SEI film, respectively. $\Delta\delta_{SEI}$ changes with the amount of new SEI film n_{SEI} generated from the lithium plating reaction and can be calculated by Eq. 24, where M_{SEI} is the molar mass of SEI film, and ρ_{SEI} is the density of SEI film

$$R_{SEI}=\frac{\delta_{SEI,0}+\Delta\delta_{SEI}}{\sigma_{SEI}} \quad [23]$$

$$\Delta\delta_{SEI}=\frac{n_{SEI}M_{SEI}}{\rho_{SEI}F} \quad [24]$$

Energy balance equations.—The change of battery temperature follows the energy balance equation, as in Eq. 25, where ρ_{bat} is the battery density, C_p is the heat capacity of the battery, and Q is the average internal heat generation and can be calculated by Eq. 26. Q_{act}, Q_{rea} and Q_{ohm} represent the active polarization heat, reaction heat and ohmic heat, and can be calculated by Eqs. 27∼29, respectively. h is the convection coefficient between the battery and ambient, a_{bat} is the specific surface area of the battery, and T_{amb} is the ambient temperature.

$$\rho_{bat}C_p\frac{\partial T}{\partial t}=Q-ha_{bat}(T_{amb}-T) \quad [25]$$

$$Q=\int_{x=0}^{L_n+L_{sep}+L_p}(Q_{act}+Q_{rea}+Q_{ohm})\,dx/\left(L_n+L_{sep}+L_p\right) \quad [26]$$

$$Q_{act}=a_sFj(\phi_s-\phi_e-U-FjR_{SEI}) \quad [27]$$

$$Q_{rea}=a_sFjT\frac{dU}{dT} \quad [28]$$

$$Q_{ohm}=\sigma_s^{eff}\left(\frac{\partial\phi_s}{\partial x}\right)^2+\sigma_e^{eff}\left(\frac{\partial\phi_e}{\partial x}\right)^2+\frac{2\sigma_e^{eff}RT}{F}(1-t_+)\frac{\partial\ln c_e}{\partial x}\frac{\partial\phi_e}{\partial x} \quad [29]$$

Temperature dependent parameters.—Some parameters in the electrochemical model are temperature dependent,[41] such as diffusion coefficient, electrical conductivity and reaction rate constant. Their values at a certain temperature T can be calculated by the Arrhenius equation:

$$Y_T=Y_{ref}\cdot\exp\left[\frac{E_{a,Y}}{R}\left(\frac{1}{T_{ref}}-\frac{1}{T}\right)\right] \quad [30]$$

where Y stands for the temperature dependent parameters, Y_{ref} is the value of the parameter at reference temperature T_{ref}, and $E_{a,Y}$ is the activation energy corresponding to the parameter Y.

Experimental

Commercial pouch lithium-ion batteries with a 24Ah nominal capacity were tested for model calibration and validation. The battery has $Li_x(NiCoMn)_{1/3}O_2$ as cathode and Li_xC_6 as anode. The batteries were tested using an 8-channel battery cycler (Neware BTS4000-5V100A). An environmental chamber (DONGGUAN BELL BE-TH-150M3) was utilized to control the ambient temperature, and temperature sensors were attached on the surface of the tested batteries to monitor temperature change.

The initial capacities of all the tested batteries were first characterized at 25°C by cycling three times at 1/3C (constant current(CC) charge to 4.2V at 1/3C and then constant voltage(CV) charge at 4.2V until current goes lower than 1/20C, discharge to 2.5V at 1/3C). The discharge capacity in the third cycle was considered as the initial capacity of the tested battery. After capacity characterization, the batteries were charged to 4.2V using CCCV charging method with different C-rates (1/6C, 1/3C, 2/3C, 1C and 2C) at 25°C to calibrate the model parameters at reference temperature. Pulse charging tests at different ambient temperatures (−5°C, 10°C, 25°C and 40°C) were then performed to extract the activation energies of the temperature dependent parameters. During the pulse charging tests, the batteries were first charged at 1C for 6min, followed by a 1.5h rest period for the batteries to reach equilibrium. The pulse charge-rest sequence was repeated until the battery voltage reaches 4.2V.

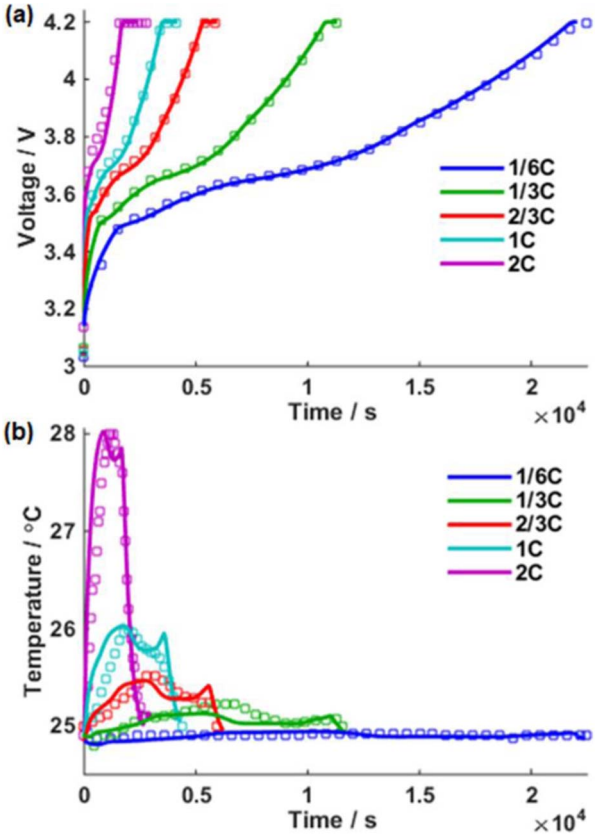

Figure 4. Validation of the electrochemical model under charging tests at 25°C, solid line = model, circle marker = experiment. (a) voltage responses at different C-rates; (b) temperature responses at different C-rates.

Low temperature charging tests were performed at −5°C to investigate the lithium plating-stripping behaviors. The batteries were charged to 4.2V using CCCV charging method with different C-rates (1/6C, 1/3C, 2/3C, 1C and 2C) to induce lithium plating, followed by a 7.5 h rest period at −5°C to ensure fully stripping of the reversible lithium. The ambient temperature was then changed to 25°C, and the batteries were cycled at 1/3C to measure the capacity degradation caused by lithium plating.

Furthermore, half cells with $Li_x(NiCoMn)_{1/3}O_2$ /Li and Li_xC_6/Li electrodes were assembled using pieces cut from the electrodes of one battery. The half-cells were cycled with C/25 current at 25°C to acquire the open circuit potential curves of cathode and anode.

Results and Discussion

The electrochemical model is established in COMSOL Multiphysics ver5.2a, with the model parameters listed in Table I. The model parameters are derived from measurements (geometric parameters) or literature, and some of them are fitted using the experimental results. The battery voltage is calculated by the following expression:

$$E_{cell}=\phi_s|_{x=L_n+L_{sep}+L_p}-\phi_s|_{x=0} \quad [31]$$

Model validation.—Model validation is carried out by comparing the simulated results with experimental data under variant conditions.

Fig. 4 compares the model results and experimental data under charging tests with different C-rates at 25°C. Both the model-predicted voltage and temperature responses can fit the experimental results well. Furthermore, the model responses under pulse charging tests at

Table I. The parameters used in the electrochemical model.

Symbol	Parameter	Unit	Value		
Constant					
F	Faraday constant	$C \cdot mol^{-1}$	96487		
R	Ideal gas constant	$J \cdot mol^{-1} \cdot K^{-1}$	8.314		
T_{ref}	Reference temperature	K	298.15		
Thermal properties					
ρ_{bat}	Density of the battery	$kg \cdot m^{-3}$	2407[a]		
C_p	Heat capacity of the battery	$J \cdot kg^{-1} \cdot K^{-1}$	1100[a]		
h	Convection coefficient	$W \cdot m^{-2} \cdot K^{-1}$	18[a]		
a_{bat}	Specific surface area of the battery	m^{-1}	277.78[a]		
Symbol	Parameter	Unit	Negative electrode	Separator	Positive electrode
Geometric parameters and volume fractions					
L	Length	m	90×10^{-6}[a]	30×10^{-6} [a]	68×10^{-6} [a]
R_s	Particle radius	m	1×10^{-6}[a]		1×10^{-6} [a]
ε_s	Volume fraction of the solid phase	1	0.471[45]		0.297[45]
ε_e	Volume fraction of the electrolyte phase	1	0.357[45]	0.45[45]	0.444[45]
a_s	Specific interfacial area	m^{-1}	$3\varepsilon_s/R_s$		$3\varepsilon_s/R_s$
Transport properties					
σ_s	Electrical conductivity in the solid phase	$S \cdot m^{-1}$	100[46]		3.8[47]
σ_s^{eff}	Effective electrical conductivity in the solid phase	$S \cdot m^{-1}$	$\varepsilon_s^{1.5}\sigma_s$		$\varepsilon_s^{1.5}\sigma_s$
$\sigma_{e,ref}$	Electrical conductivity in the electrolyte phase at T_{ref}	$S \cdot m^{-1}$	$c_e(5.38 - 3.49 \times 10^{-4}c_e + 2.30 \times 10^{-7}c_e^2)^2 \times 10^{-4}$[48]		
E_{a,σ_e}	Activation energy for σ_e	$kJ \cdot mol^{-1}$	30[c]		
σ_s^{eff}	Effective electrical conductivity in the electrolyte phase	$S \cdot m^{-1}$	$\varepsilon_e^{1.5}\sigma_e$	$\varepsilon_e^{1.5}\sigma_e$	$\varepsilon_e^{1.5}\sigma_e$
$c_{e,0}$	Initial value of Li^+ concentration in the electrolyte phase	$mol \cdot m^{-3}$	1200[c]		
$c_{s,max}$	Maximum solid phase Li^+ concentration	$mol \cdot m^{-3}$	27872[c]		85187[c]
D_s	Solid phase diffusion coefficient	$m^2 \cdot s^{-1}$	3.9×10^{-14}[46]		4.5×10^{-13}[47]
$D_{e,ref}$	Electrolyte phase diffusion coefficient at T_{ref}	$m^2 \cdot s^{-1}$	$10^{-8.43-54/(59.15-0.005c_e)-2.2\times10^{-4}c_e^2}$[48]		
E_{a,D_e}	Activation energy for D_e	$kJ \cdot mol^{-1}$	72[c]		
D_e^{eff}	Effective electrolyte phase diffusion coefficient	$m^2 \cdot s^{-1}$	$\varepsilon_e^{1.5}D_e$	$\varepsilon_e^{1.5}D_e$	$\varepsilon_e^{1.5}D_e$
x	Stoichiometry coefficient, x at 1, 0 SOC	1	0.8911, 0.0373[c]		0.3585, 0.9448[c]
t_+	Transference number	1	0.382[45]		

Table I. The parameters used in the electrochemical model.

Symbol	Parameter	Unit	Value	
Kinetics parameters				
$\alpha_{a,1}$, $\alpha_{c,1}$	Transfer coefficients of lithium intercalation reaction	1	0.5, 0.5[26]	0.5, 0.5[26]
$k_{1,ref}$	Reaction rate constant of lithium intercalation reaction at T_{ref}	$m^{2.5} \cdot mol^{-0.5} \cdot s^{-1}$	3.5×10^{-11} [c]	9×10^{-11} [c]
E_{a,k_1}	Activation energy for k_1	$kJ \cdot mol^{-1}$	71[c]	45[c]
U_{ref}	Open circuit potential at T_{ref}	V	Fig. 3a[a]	Fig. 3b[a]
$\frac{dU}{dT}$	Entropic heat coefficient	$V \cdot K^{-1}$	Fig. 3a[46]	Fig. 3b[47]
$\alpha_{a,2}$, $\alpha_{c,2}$	Transfer coefficients of lithium plating and stripping reactions	1	0.3, 0.7[26]	
$k_{2,ref}$	Reaction rate constant of lithium plating and stripping reactions at T_{ref}	$mol^{0.7} \cdot m^{-1.1} \cdot s^{-1}$	3.0×10^{-6} [c]	
E_{a,k_2}	Activation energy for k_2	$kJ \cdot mol^{-1}$	50[c]	
U_{Li}	Equilibrium potential of lithium plating reaction	V	0[26]	
z_1,z_2,z_3	Fractions of reversible lithium, dead lithium and SEI film generated from lithium plating reaction	1	0.775, 0.175, 0.05[c]	
β	Correction parameter of lithium stripping reaction	1	1000[c]	
$\delta_{SEI,0}$	Initial thickness of the SEI film	m	1×10^{-9} [c]	0
σ_{SEI}	Electrical conductivity of the SEI film	$S \cdot m^{-1}$	5×10^{-6}[49]	
M_{SEI}	Molar mass of SEI film	$kg \cdot mol^{-1}$	0.162[49]	
ρ_{SEI}	Density of SEI film	$kg \cdot m^{-3}$	1690[49]	

[a]The geometric parameters, the thermal and electrochemical properties of the 24Ah battery are derived from measurements.
[b]The parameters that have citations are derived from the cited literature.
[c]The parameters that have no citations are evaluated within practical ranges to fit the experimental data.

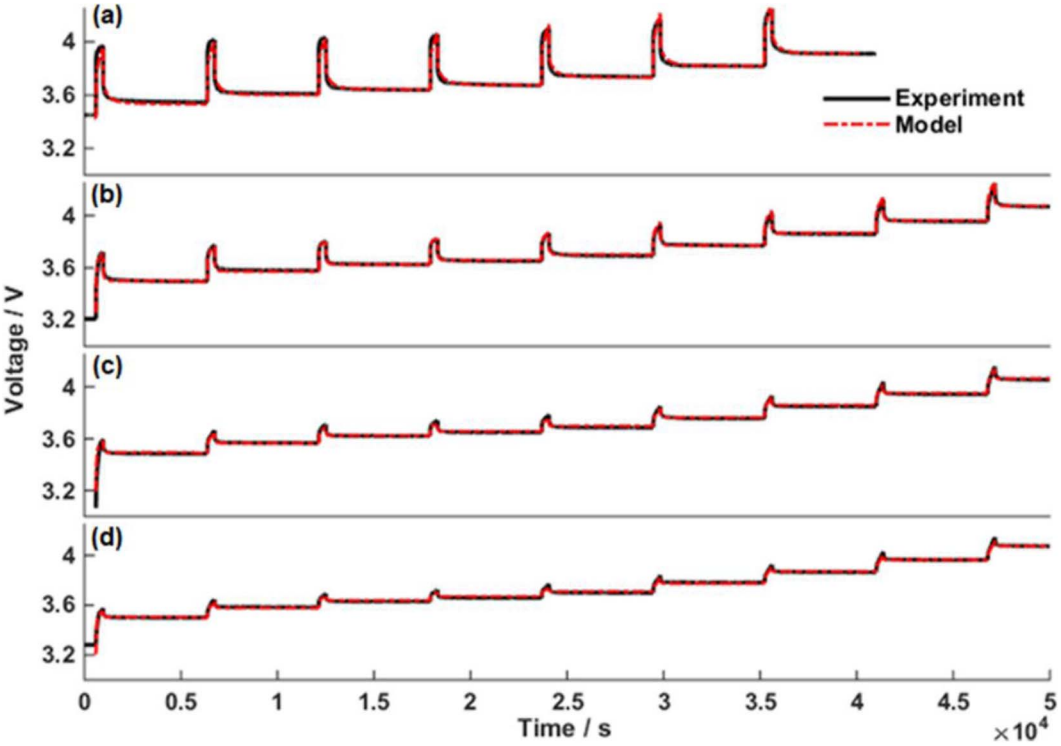

Figure 5. Model validation under pulse charging tests at variant temperature. (a) −5°C; (b) 10°C; (c) 25°C; (d) 45°C.

four different temperatures are also consistent with the experimental data, as shown in Fig. 5, indicating that the electrochemical model has adequate accuracy.

The model is further applied to study the battery performance at low temperature. The voltage and temperature responses of the batteries charged at −5°C are compared in Fig. 6, where the *x* axis has been changed from time to charged capacity to better illustrate the battery performance. The simulated battery voltage profiles can fit the experimental results well at differential C-rates, as presented in Fig. 6a, except for the deviation at beginning of 2C charging. The deviation mainly results from the decrease of solid phase diffusion coefficients at low SOC,[42] while the solid phase diffusion coefficients are considered as SOC independent in this study. The simulated temperature responses also agree well with the experimental data, as show in Fig. 6b, convincing us that the model can predict the electrochemical and thermal performance of the battery at low temperature well.

Voltage plateau during the rest period after low temperature charging have been considered as a characteristic signature of the lithium stripping process.[15,24,43] In this study, the batteries were rested at −5°C for 7.5 h after low temperature charging to investigate the lithium stripping behaviors. Fig. 7 presents the simulated and experimental voltage relaxation behaviors after charging tests at −5°C. The model results exhibit similar voltage relaxation behaviors as the experimental data despite some deviations in the shape of voltage curves. Distinctive voltage plateaus were found in both simulated and experimental voltage relaxation profiles of the batteries charged at currents higher than 1/3C, while the battery charged at 1/6C shows exponentially decreasing voltage during rest period. To the best of the authors' knowledge, that is the first electrochemical model that successfully predicts the characteristic voltage plateau in the relaxation period after lithium plating.

Capacity losses induced by low temperature charging were evaluated by cycling the batteries with a current of 1/3C at 25°C, as presented in Table II. The batteries charged with currents larger than 1/3C exhibit obvious capacity loss, indicating significant lithium plating in the batteries, while the battery charged at 1/6C shows little capacity loss and plated lithium. The model can achieve a

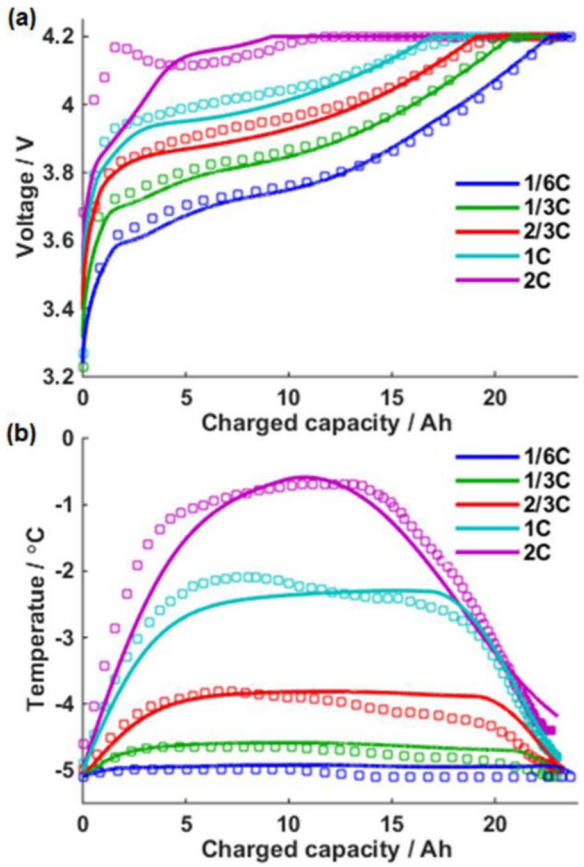

Figure 6. Comparison of the model results and experimental data under charging tests at −5°C, solid line = model, circle marker = experiment. (a) voltage responses at variant C-rates; (b) temperature responses at variant C-rates.

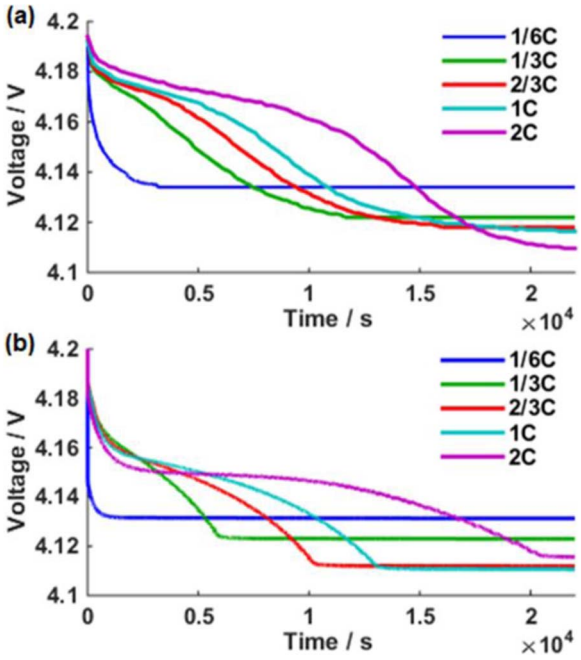

Figure 7. Comparison of the voltage relaxation behaviors after charging at −5°C. (a)experiment; (b) model.

Table II. Comparison of the simulated and experimental capacity loss of the batteries charged at −5°C.

	Capacity loss / %	
Charge current rate	Experiment	Model
1/6C	0	0.064
1/3C	1.672	1.996
2/3C	3.780	3.631
1C	5.577	5.105
2C	8.845	7.240

reasonable prediction of battery degradation behaviors induced by lithium plating, as the predicted capacity degradations are consistent with the experimental data.

Origin of the characteristic voltage plateau during the rest period.—As shown in Fig. 7, a characteristic plateau can sometimes be found in the battery voltage relaxation curves after low temperature charging. Several researchers have taken the voltage plateau as an indicator of the lithium stripping process.[15,24,43] However, little direct evidence has been presented to correlate the voltage plateau with lithium stripping behaviors due to the difficulties in observation of lithium stripping reaction. In this study, detailed analysis of the lithium stripping process is carried out based on the validated electrochemical model.

The changes of anode potential at anode/separator interface and anode/current collector interface during the rest period after low temperature charging are presented in Figs. 8a and 8b. Distinctive plateaus are observed in the anode potential profiles at both anode/separator interface and anode/current collector interface for the batteries charged with currents larger than 1/3C, like the battery voltage plateaus. As shown in Fig. 8c, for the battery charged at a 1/6C with tiny plated lithium, the lithium content at anode surface keeps decreasing during the rest period due to diffusion; while rapid increases of the lithium content are found at the anode/separator interface of the batteries charged with currents larger than 1/3C, resulting from lithium stripping and re-intercalation reactions. The lithium content begins to decrease after peaking at a high value, and turning point that indicates the fully consumption of the reversible lithium, is consistent with the end of potential plateau shown in Fig. 8a. Similar difference in the changes of lithium content at anode/current collector interface between the batteries charged with currents higher 1/3C and with a 1/6C current can also be found in Fig. 8d. Lithium content at anode/current collector interface for the batteries charged with currents higher 1/3C increases rapidly, while that for the battery charged at 1/6C keeps almost constant during the whole rest period. The increase of lithium content at anode surface will change the electrical potential in the solid phase $\phi_s|_{x=0}$, resulting in further changes in battery voltage according to Eq. 31. Therefore, we can conclude that the plateau in the voltage relaxation profiles after lithium plating is induced by lithium stripping and re-intercalation reactions at anode surface, and the end of the voltage plateau has correlations with the full consumption of the reversible plated lithium.

Detection of lithium plating via differential voltage analysis.—Differential voltage analysis is an effective tool to reveal the electrochemical reactions in lithium ion battery.[44] In this study, a modified differential voltage analysis with respect to time is applied to investigate the lithium stripping process, as presented in Fig. 9. Distinct local minima can be found in the differential voltage curves of the batteries charged with currents higher than 1/3C, while that of the battery charged at 1/6C rises exponentially, as shown in Fig. 9b. The positions of the local minima are identified as the points in time, denoted as $t_{\min}$. $t_{\min}$ increases with charging current and correlates to the fully stripping of the reversible lithium, as presented in Fig. 9c. The relationship between the total amount of reversible lithium $N_{\text{Li,rev}}$ and $t_{\min}$ is further presented in Fig. 10, where a good linear relationship can be observed and fitted by Eq. 32. As a result, $t_{\min}$ determined by the differential analysis on the voltage plateau can be used as a quantitative indicator for the amount of reversible lithium.

$$N_{\text{Li,rev}} = 1.2367 \times 10^{-5} \cdot t_{\min} + 0.0035 \quad [32]$$

Influence of ambient temperature on lithium plating detection.—The electrochemical model is further applied to simulate the lithium plating-stripping process in lithium-ion battery at varying temperature. The voltage relaxation behaviors of the batteries charged at −10°C and 0°C are presented in Figs. 11a and 11b, respectively. Similar plateaus can be found in the voltage relaxation profiles of the batteries charged at −10°C and 0°C, and characteristic local minima can also be seen in the differential voltage curves shown in Figs. 11c and 11d. The total amount of reversible lithium $N_{\text{Li,rev}}$ in relation to $t_{\min}$ in the differential voltage curves at different ambient temperatures is compared in Fig. 12. Good linear relationships between $N_{\text{Li,rev}}$ and $t_{\min}$ are observed in all the three simulated results, with the fitting equations presented in Eq. 33, indicating that quantitative detection of lithium plating based on the differential voltage analysis can work well at variant temperatures. Furthermore, for the battery with the same amount of reversible lithium, the time required for fully stripping of reversible lithium, i.e. $t_{\min}$, increases when lowering the ambient temperature, due to the decrease of lithium stripping reaction rate.

$$N_{\text{Li,rev}} = \begin{cases} 2.4090 \times 10^{-5} \cdot t_{\min} - 0.0051, T_{\text{amb}} = 0°\text{C} \\ 1.2367 \times 10^{-5} \cdot t_{\min} + 0.0035, T_{\text{amb}} = -5°\text{C} \\ 6.6363 \times 10^{-6} \cdot t_{\min} + 0.0180, T_{\text{amb}} = -10°\text{C} \end{cases} \quad [33]$$

Influence of rest time on lithium plating detection.—The quantitative detection of lithium plating based on the differential analysis on the voltage relaxation behaviors requires a rest period of several hours for the fully stripping of reversible lithium, as shown in Fig. 9 and Fig. 11, while the rest duration during cycling tests or real-time operation is usually shorter than 1 hour. Some researchers have proposed similar quantitative detection methods for lithium plating via differential analysis on the discharge voltage profiles after low temperature charging.[24,25] However, the quantitative relationship has not been proved and the effect of rest time is still unclear.

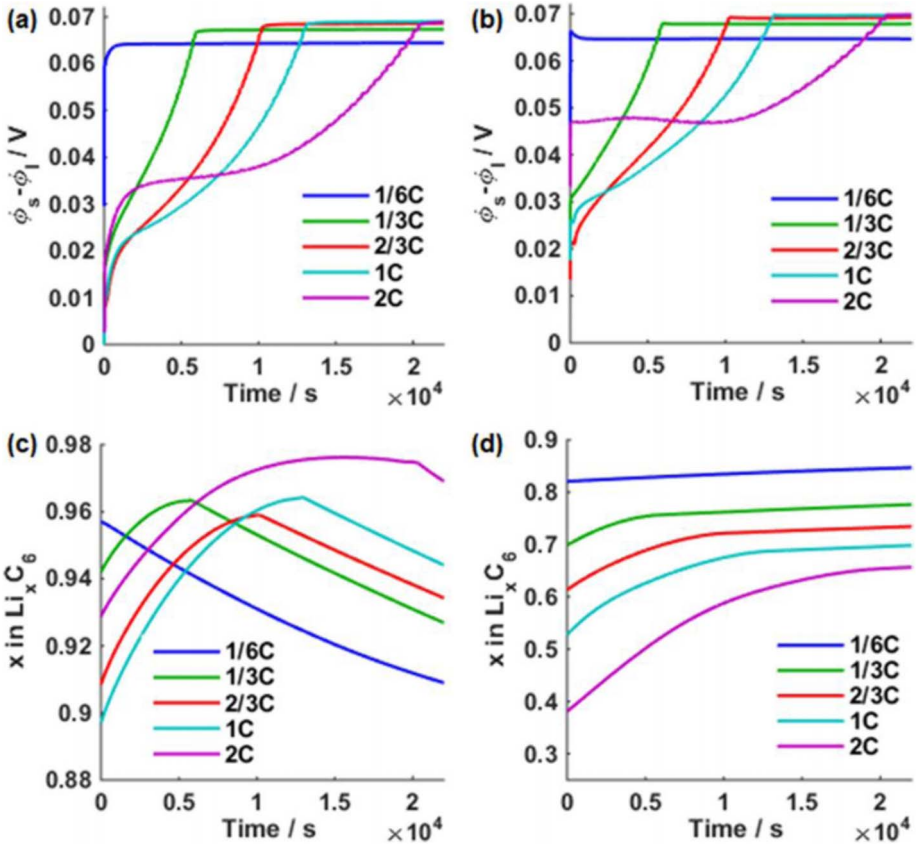

Figure 8. Changes of anode potential and lithium content at anode surface during the rest period. (a) and (b) changes of anode potential at anode/separator interface and anode/current collector interface, respectively; (c) and (d) changes of lithium content at anode/separator interface and anode/current collector interface, respectively.

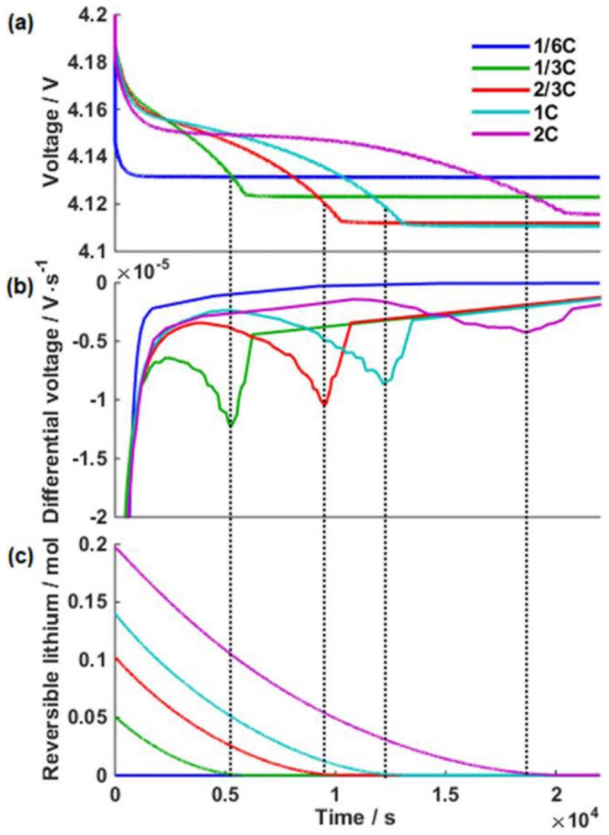

Figure 9. Differential analysis on the voltage relaxation behaviors. (a) battery voltage relaxation profiles; (b) differential voltage analysis; (c) change of the amount of reversible lithium.

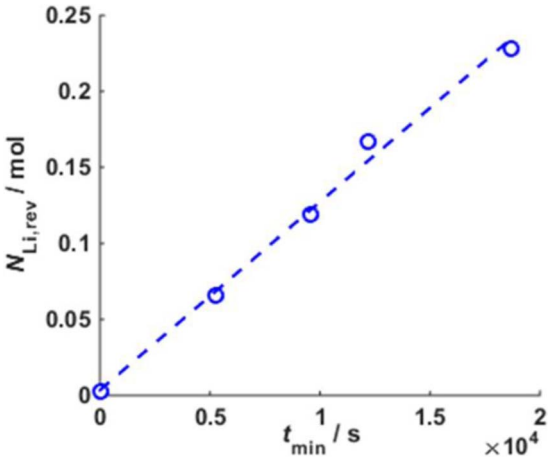

Figure 10. The relationship between $N_{\mathrm{Li,rev}}$ and t_{min}, circle marker = model results, dash line = fitting.

In this study, simulation based on the electrochemical model is carried out to investigate the influence of rest time on detection of lithium plating. The batteries were first fully charged with different current rates at −5°C, and then rested for different lengths of time (t_{rest} = 0min, 30min and 60min), followed by discharged to 2.5V with a current of 1/3C at −5°C. The batteries voltage profiles during rest and discharge periods are presented in Fig. 13, where three different lengths of rest period are compared. While the voltage plateau is difficult to identify by eye from the discharge voltage curves, differential analysis on the discharge voltage profiles shows distinct local minima, as shown in Fig. 14. The position of the local minima in the differential voltage curves is denoted as $t_{\mathrm{min,dch}}$. As shown in Figs. 14a∼14c, $t_{\mathrm{min,dch}}$ increases with charging current in all the three simulation cases with different rest time, the same trend as that in

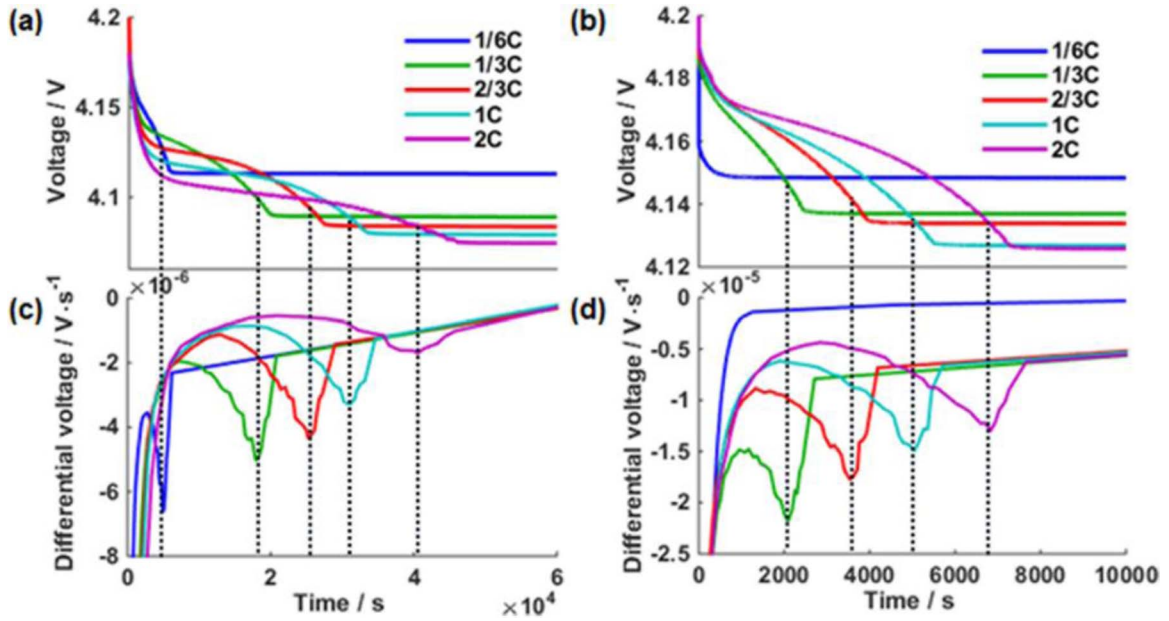

Figure 11. The voltage relaxation behaviors of the batteries charged at −10°C and 0°C. (a) and (b) voltage relaxation profiles of the batteries charged at −10°C, 0°C, respectively; (c) and (d) differential analysis on the voltage relaxation profiles at −10°C, 0°C, respectively.

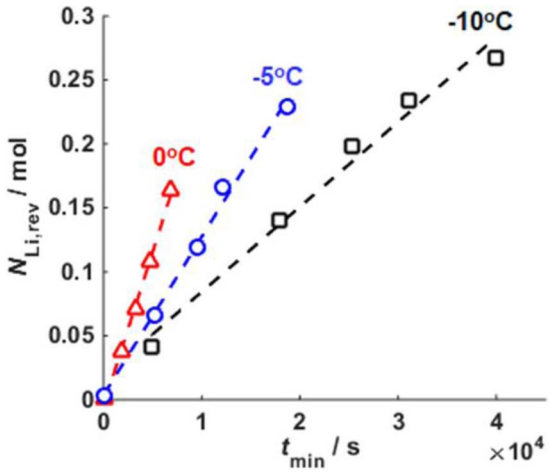

Figure 12. The relationship between $N_{Li,rev}$ and t_{min} at variant ambient temperatures, circle marker = model results, dash line = fitting.

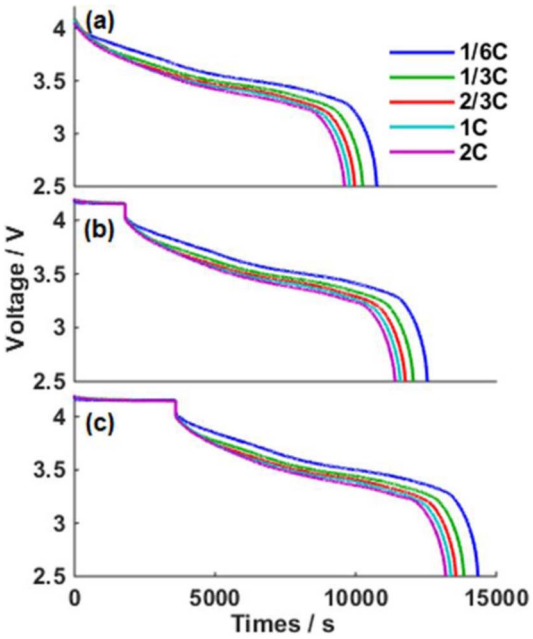

Figure 13. Relaxation and discharge voltage profiles of the batteries charged at −5°C and rest for different lengths of time. (a) t_{rest} = 0min; (b) t_{rest} = 30min; (c) t_{rest} = 60min.

Fig. 9 and Fig. 11, indicating that $t_{min,dch}$ can also be trusted as an indicator for the amount of reversible lithium. For battery charged at a same current, $t_{min,dch}$ decreases with the increase of rest time, as part of the reversible lithium have stripped into electrolyte during the rest period.

The amount of reversible lithium $N_{Li,rev}$ in relation to $t_{min,dch}$ is presented in Fig. 15. For the battery discharged immediately after low temperature charging (t_{rest} = 0min), linear relationship between $N_{Li,rev}$ and $t_{min,dch}$ is observed and can be fitted by Eq. 34; for the battery discharged after rest for a while (t_{rest} = 30min and 60min), the amount of reversible lithium stripped during rest period can be calculated by Eq. 32, while that stripped during discharge process is calculated by Eq. 34, thus the total amount of reversible lithium $N_{Li,rev}$ can be calculated by Eq. 35. The amount of reversible lithium calculated by Eq. 35 is compared with the simulation results in Fig. 15 and shows to be in good agreement. As a result, the time of the local minima in the differential discharge voltage curves can also be used as a quantitative indicator for the amount of reversible lithium.

$$N_{Li,rev} = 7.2177 \times 10^{-5} \cdot t_{min,dch} - 0.0044 \quad [34]$$

$$N_{Li,rev} = \left(1.2367 \times 10^{-5} \cdot t_{rest} + 0.0035\right) + \left(7.2177 \times 10^{-5} \cdot t_{min,dch} - 0.0044\right) \quad [35]$$

Conclusions

In this paper, an electrochemical model with lithium plating and stripping reactions incorporated as side reactions at the anode surface

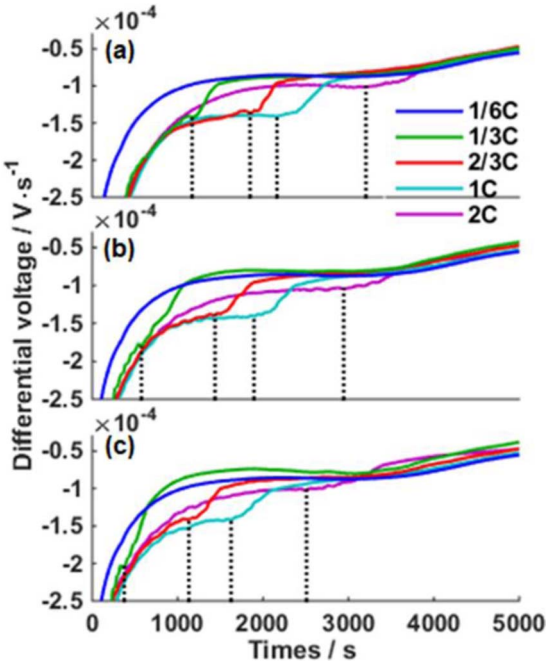

Figure 14. Differential analysis on the discharge voltage profiles of the batteries charged at −5°C and rest for different lengths of time. (a) t_{rest} = 0min; (b) t_{rest} = 30min; (c) t_{rest} = 60min.

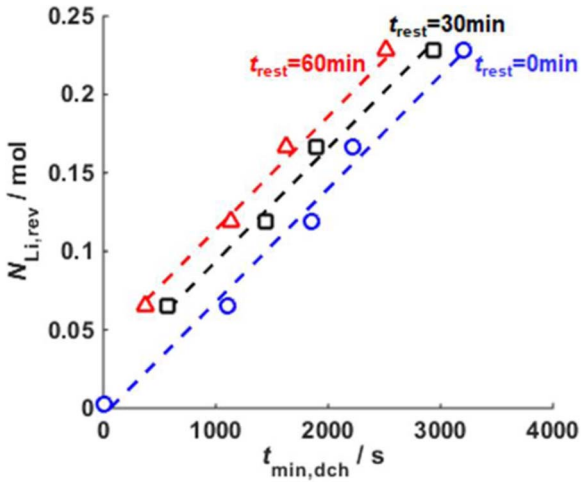

Figure 15. The relationship between $N_{Li,rev}$ and $t_{min,dch}$ for the battery discharged after rest for different t_{rest}, circle marker = model results, dash line = calculation by Eq. 35.

is built to explore the lithium plating-stripping behaviors in lithium-ion batteries at low temperature. The model is validated through a series of experiments on a 24Ah commercial lithium-ion battery and shows good accuracy. Furthermore, the model can successfully simulate the characteristic plateau in the battery voltage relaxation profiles after low temperature charging. The model-predicted capacity loss induced by lithium plating with different C-rates is also consistent with experimental data, indicating that the model can predict the lithium plating and stripping behaviors at low temperature well.

Modeling analysis is performed to reveal the origin of the characteristic voltage plateau. Similar plateaus are also observed in the anode potential profiles during the rest period after low temperature charging, along with the increase of lithium content at anode surface, convincing us that the voltage plateau is induced by lithium stripping and re-intercalation reactions at anode surface. Moreover, the end of the voltage plateaus is found to correlate with the full consumption of the reversible lithium.

Quantitative detection of lithium plating via differential analysis on the voltage relaxation profiles is discussed using the validated model. Distinct local minima can be found in the differential voltage curves. The positions of the local minima t_{min} increase with charging current and correlate to the fully stripping of the reversible lithium. A linear relationship between the total amount of reversible lithium $N_{Li,rev}$ and t_{min} is observed, indicating that t_{min} can be used as a quantitative indicator for the amount of reversible lithium. The effect of ambient temperature on the detection of lithium plating is further analyzed, and good linear relationships between $N_{Li,rev}$ and t_{min} are observed at three different temperatures, verifying the detection method for lithium plating at a wide temperature range. The detection of lithium plating via differential voltage analysis is further extended to discharge voltage profiles of the batteries charged at low temperature considering the effect of rest time. An equation combining the reversible lithium stripped in the rest and discharge period is proposed to estimate the amount of reversible lithium and shows good agreement.

Acknowledgment

This work is supported by the National Natural Science Foundation of China under the grant No. U1564205 and No.51706117, the Ministry of Science and Technology of China under the grant No. 2016YFE0102200, and the Beijing Natural Science Foundation under the grant No.3184052. The first author appreciates the funding from China Scholarship Council. This work was authored in part by Alliance for Sustainable Energy, LLC, the Manager and Operator of the National Renewable Energy Laboratory for the U.S. Department of Energy (DOE) under Contract No. DE-AC36-08GO28308. Funding for the second author was provided by U.S. Department of Energy Office of Energy Efficiency and Renewable Energy Vehicle Technologies Office, program manager Samuel Gillard. The views expressed in the article do not necessarily represent the views of the DOE or the U.S. Government. The U.S. Government retains and the publisher, by accepting the article for publication, acknowledges that the U.S. Government retains a nonexclusive, paid-up, irrevocable, worldwide license to publish or reproduce the published form of this work, or allow others to do so, for U.S. Government purposes.

ORCID

Dongsheng Ren https://orcid.org/0000-0002-8764-9819
Kandler Smith https://orcid.org/0000-0001-7011-0377
Xuning Feng https://orcid.org/0000-0002-5790-5164

References

1. L. Lu, X. Han, J. Li, J. Hua, and M. Ouyang, *J. Power Sources*, **226**, 272 (2013).
2. P. Arora, R. E. White, and M. Doyle, *J. Electrochem. Soc.*, **145**, 3647 (1998).
3. T. Waldmann, B.-I. Hogg, and M. Wohlfahrt-Mehrens, *J. Power Sources*, **384**, 107 (2018).
4. X. Han, M. Ouyang, L. Lu, J. Li, Y. Zheng, and Z. Li, *J. Power Sources*, **251**, 38 (2014).
5. Z. Li, J. Huang, B. Yann Liaw, V. Metzler, and J. Zhang, *J. Power Sources*, **254**, 168 (2014).
6. M. Ouyang, Z. Chu, L. Lu, J. Li, X. Han, X. Feng, and G. Liu, *J. Power Sources*, **286**, 309 (2015).
7. A. Friesen, F. Horsthemke, X. Mönnighoff, G. Brunklaus, R. Krafft, M. Borner, T. Risthaus, M. Winter, and F. M. Schappacher, *J. Power Sources*, **334**, 1 (2016).
8. M. Börner, A. Friesen, M. Grutzke, Y. P. Stenzel, G. Brunklaus, J. Haetge, S. Nowak, F. M. Schappacher, and M. Winter, *J. Power Sources*, **342**, 382 (2017).
9. T. Waldmann and M. Wohlfahrt-Mehrens, *Electrochim. Acta*, **230**, 454 (2017).
10. X. Feng, X. He, L. Lu, and M. Ouyang, *J. Electrochem. Soc.*, **165**, A155 (2018).
11. X. Feng, M. Ouyang, X. Liu, L. Lu, Y. Xia, and X. He, *Energy Storage Mater.*, **10**, 246 (2018).
12. B. V. Ratnakumar and M. C. Smart, *ECS Trans.*, **25**, 241 (2010).
13. M. Ecker, P. Shafiei Sabet, and D. U. Sauer, *Appl. Energy*, **206**, 934 (2017).
14. T. Waldmann, B. I. Hogg, M. Kasper, S. Grolleau, C. G. Couceiro, K. Trad, B. P. Matadi, and M. Wohlfahrt-Mehrens, *J. Electrochem. Soc.*, **163**, A1232 (2016).

15. C. von Lüders, V. Zinth, S. V. Erhard, P. J. Osswald, M. Holfmann, R. Gilles, and A. Jossen, *J. Power Sources*, **342**, 17 (2017).
16. V. Zinth, C. von Lüders, M. Holfmann, J. Hattendorff, I. Buchberger, S. Erhard, J. Rebelo-Kornmeier, A. Jossen, and R. Gilles, *J. Power Sources*, **271**, 152 (2014).
17. J. Arai and R. Nakahigashi, *J. Electrochem. Soc.*, **164**, A3403 (2017).
18. K. Gotoh, M. Izuka, J. Arai, Y. Okada, T. Sugiyama, K. Takeda, and H. Ishida, *Carbon N. Y.*, **79**, 380 (2014).
19. J. Arai, Y. Okada, and K. Gotoh, *J. Electrochem. Soc.*, **162**, A952 (2015).
20. J. Wandt, P. Jakes, J. Granwehr, R.-A. Eichel, and H. A. Gasteiger, *Mater. Today*, **21**, 231 (2018).
21. N. Legrand, B. Knosp, P. Desprez, F. Lapicque, and S. Raël, *J. Power Sources*, **245**, 208 (2014).
22. S. Ahmed, I. Bloom, A. N. Jansen, T. Tanim, E. J. Dufek, A. Pesaran, A. Burnham, R. B. Carlson, F. Dias, K. Hardy, M. Keyser, C. Kreuzer, A. Markel, A. Meintz, C. Michelbacher, M. Mohanpurkar, P. A. Nelson, D. C. Robertson, D. Scoffield, M. Shirk, T. Stephens, R. Vijayagopal, and J. Zhang, *J. Power Sources*, **367**, 250 (2017).
23. M. Ouyang, D. Ren, L. Lu, J. Li, X. Feng, X. Han, and G. Liu, *J. Power Sources*, **279**, 626 (2015).
24. S. Schindler, M. Bauer, M. Petzl, and M. A. Danzer, *J. Power Sources*, **304**, 170 (2016).
25. M. Petzl and M. A. Danzer, *J. Power Sources*, **254**, 80 (2014).
26. P. Arora, M. Doyle, and R. E. White, *J. Electrochem. Soc.*, **146**, 3543 (1999).
27. M. Doyle, T. F. Fuller, and J. Newman, *J. Electrochem. Soc.*, **140**, 1526 (1993).
28. M. Doyle and J. Newman, *J. Electrochem. Soc.*, **143**, 1890 (1996).
29. M. Tang, P. Albertus, and J. Newman, *J. Electrochem. Soc.*, **156**, A390 (2009).
30. S. Tippmann, D. Walper, L. Balboa, B. Spier, and W. G. Bessler, *J. Power Sources*, **252**, 305 (2014).
31. H. Ge, T. Aoki, N. Ikeda, S. Suga, T. Isobe, Z. Li, Y. Tabuchi, and J. Zhang, *J. Electrochem. Soc.*, **164**, A1050 (2017).
32. X. G. Yang, Y. Leng, G. Zhang, S. Ge, and C. Y. Wang, *J. Power Sources*, **360**, 28 (2017).
33. S. Santhanagopalan, Q. Guo, P. Ramadass, and R. E. White, *J. Power Sources*, **156**, 620 (2006).
34. R. D. Perkins, A. V. Randall, X. Zhang, and G. L. Plett, *J. Power Sources*, **209**, 318 (2012).
35. Z. Chu, X. Feng, L. Lu, J. Li, X. Han, and M. Ouyang, *Appl. Energy*, **204**, 1240 (2017).
36. X. Han, M. Ouyang, L. Lu, and J. Li, *J. Power Sources*, **278**, 802 (2015).
37. X. Han, M. Ouyang, L. Lu, and J. Li, *J. Power Sources*, **278**, 814 (2015).
38. A. M. Colclasure, K. A. Smith, and R. J. Kee, *Electrochim. Acta*, **58**, 33 (2011).
39. R. Spotnitz and J. Franklin, *J. Power Sources*, **113**, 81 (2003).
40. D. Ren, X. Feng, L. Lu, M. Ouyang, S. Zheng, J. Li, and X. He, *J. Power Sources*, **364**, 328 (2017).
41. M. Guo, G. Sikha, and R. E. White, *J. Electrochem. Soc.*, **158**, A122 (2011).
42. A. Verma, K. Smith, S. Santhanagopalan, D. Abraham, K. P. Yao, and P. P. Mukherjee, *J. Electrochem. Soc.*, **164**, A3380 (2017).
43. Waldmann, J. B. Quinn, K. Richter, M. Kasper, A. Tost, A. Klein, and M. Wohlfahrt-Mehrens, *J. Electrochem. Soc.*, **164**, A3154 (2017).
44. I. Bloom, A. N. Jansen, D. P. Abraham, J. Knuth, S. A. Jones, V. S. Battaglia, and G. L. Henriksen, *J. Power Sources*, **139**, 295 (2005).
45. 1D Isothermal Lithium-Ion Battery. User manual of COMSOL Multiphysics, ver 5.2a; 2016.
46. Material property for Li_xC_6 MCMB electrode material of COMSOL Multiphysics, ver 5.2a; 2016.
47. Material property for $LiNi_{1/3}Mn_{1/3}Co_{1/3}O_2$ electrode material of COMSOL Multiphysics, ver 5.2a; 2016.
48. L. O. Valo/en and J. N. Reimers, *J. Electrochem. Soc.*, **152**, A882 (2005).
49. M. Safari, M. Morcrette, A. Teyssot, and C. Delacourt, *J. Electrochem. Soc.*, **156**, A145 (2009).